Modulating image oscillations in focusing by a metamaterial lens: Time-dependent Green's function approach

Xueqin Huang and Lei Zhou*
Surface Physics Laboratory (State Key Laboratory) and Physics Department, Fudan University, Shanghai 200433, People's Republic of China

C. T. Chan
Physics Department, Hong Kong University of Science and Technology, Clear Water Bay, Kowloon, Hong Kong, China
(Received 25 December 2005; revised manuscript received 27 May 2006; published 25 July 2006)

It was demonstrated previously that the image focused with an $\varepsilon=\mu=-1$ metamaterial lens is intrinsically unstable, and adding absorption stabilizes the image at the price of degrading the image resolution. Here we show that a stable image with the highest possible resolution can be obtained in the shortest duration, if the source's "switching-on" time matches the intrinsic focusing speed of the lens. We demonstrate that the image oscillations, although appearing different and complicated in different situations, are *all* dictated by the interactions between the source spectra and the lens surface modes, and can be efficiently modulated by the lens thickness and the material parameters.

DOI: 10.1103/PhysRevB.74.045123 PACS number(s): 78.20.Ci., 42.30.−d, 42.50.Md, 41.20.Jb

I. INTRODUCTION

A conventional optical lens cannot form a subwavelength image with resolution better than half-wavelength (i.e., the diffraction limit), since the evanescent components of the source containing the higher-resolution information cannot be collected and reconstructed by a conventional lens. Veselago first proposed in 1968 that a flat metamaterial slab with $\varepsilon=\mu=-1$ could function as a lens to focus electromagnetic (EM) waves,[1] and Pendry later pointed out that this lens is actually a "perfect" one, with imaging ability unbounded by the usual diffraction limit.[2] People soon realized that $\varepsilon(\mu)$ should have a small deviation (denoted by Δ, which is general complex) from -1, since otherwise the field will diverge at the exit interface of the lens.[3] Due to the presence of Δ, the image formed with such a lens is no longer perfect, but still beat the diffraction limit if Δ is sufficiently small,[4,5] so that such a lens is usually called a "super" lens.

Many studies were performed to study the perfect or super lens focusing, employing either finite-difference–time-domain (FDTD) simulations[6–11] or theoretical analyses.[12–14] Most of them were interested only in the properties of the stabilized images,[6–13] but neglected the transient behaviors in the imaging processes. However, the latter were found quite rich and intriguing in such optical processes, different from a conventional lensing problem. A pioneering FDTD simulation in a two dimensional (2D) configuration (employing an infinite line current source) showed that the fields varied dramatically over time, and no steady foci were found in focusing with a *perfect* or nearly perfect lens ($\Delta\sim10^{-9}$).[6] Later, FDTD researchers found that stable images could be achieved *only* when finite absorption was added,[7–10] and further identified such image instability as a characteristic oscillation with a definite frequency.[8] Recently, we applied a time-dependent Green's function (TDGF) approach to study the image oscillations in metamaterial lens focusing.[15,16] Our results revealed that a vortexlike transient surface mode is responsible for the oscillations in the 2D focusing[15] and the oscillating behaviors strongly depend on the dimensionality of the problem, material parameter Δ (both its real part denoted by δ, and its imaginary part), and the lens thickness, etc.[15,16] Since the vortexlike surface mode does not transport energy,[15] the resulting oscillation can only be damped out by the absorption, which naturally explained the observations of previous simulations.[6–8]

In practice, we are then facing an awkward dilemma—while absorption helps us to stabilize the image, it greatly degrades the achieved image resolution at the same time.[5] Also, we note that different situations may yield completely different types of image oscillations.[15,16] Such complexities make the instability problems difficult to handle in practical applications. In this paper, we apply the TDGF approach[15,16] to examine the instability problems in a way as general as possible, with the aim to sort out the essential physical elements that control the image oscillations, so as to help people effectively handle those image instabilities in future applications. This paper is organized as follows. In the next section, we show that strong oscillations can be suppressed via tuning the "switching-on" time, without adding more absorption to *degrade the image resolution*, and there exists an optimum value of switching-on time to achieve the *fastest* image stabilization. In Sec. III, we study the image instabilities in a complete set of linearly independent situations, and demonstrate that the transient behaviors are *all* dictated by the interactions between the source spectra and the lens surface modes, although they behave quite differently at first glance. In Sec. IV, we further analyze that the image oscillations, contributed essentially by two types of surface modes, can be respectively tuned by the lens thickness d and material parameter δ. Finally, we summarize our results in the last section.

II. THE ROLE OF THE SWITCHING-ON TIME

Although previous FDTD simulations adopted diverse and complicated switching-on processes,[6–11] a detailed

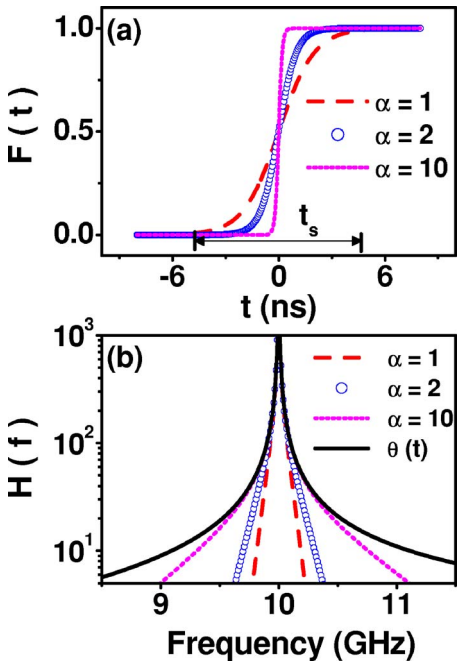

FIG. 1. (Color online) Curves of (a) $F(t)$ and (b) $H(\omega)$ with different values of α (in units of GHz). Here t_s denotes the switching-on time for $\alpha=1$ GHz case.

analysis of the role of the switching-on time is highly desirable. In this section, taking the 2D focusing as a concrete example, we employ the TDGF approach to examine the role of the switching-on time in the transient physics. The geometry is the same as in Ref. 15 so we will not repeat it here. In our previous studies,[15,16] we assumed the switching-on process as a simple step function $\theta(t)$, with a zero switching-on time. In practice, however, it seems more realistic to assume that the source field gradually develops from 0 to 1 in the switching-on process. We thus adopt the following function,

$$F(t) = \frac{1}{1+e^{-\alpha t}}, \tag{1}$$

to model this realistic situation. We note that $F(t)$ increases gradually from 0 to 1 as time increases, and the parameter α controls the transition speed, as shown in Fig. 1(a). In the limit of $\alpha \to \infty$, we find that $F(t) \to \theta(t)$, recovering the previous situation.[15,16] Let us define a parameter t_s, which is the time interval between time instances at $F=1\%$ and $F=99\%$, to quantitatively measure the switching-on time. A simple calculation shows that $t_s = 2\ln(99)/\alpha$, indicating that a larger α corresponds to a faster switching-on process with a shorter switching-on time, and vise versa. The current source is then written as

$$\vec{J}(\vec{r},t) = \hat{y} I_0 \delta(x)\delta(z) e^{-i\omega_0 t} F(t), \tag{2}$$

where ω_0 is the working frequency. Following the TDGF approach,[15] we find that the time-dependent E field can be written as

$$\vec{E}(\vec{r},t) = \frac{1}{2\pi}\int d\omega e^{-i\omega t}\vec{E}(\vec{r},\omega)H(\omega), \tag{3}$$

where

$$H(\omega) = \frac{2\pi\omega}{\alpha}\frac{e^{-\pi(\omega-\omega_0+i\eta)/\alpha}}{1-e^{-2\pi(\omega-\omega_0+i\eta)/\alpha}}, \tag{4}$$

and $\vec{E}(\vec{r},\omega) = -\mu_0 I_0 \int \vec{\vec{G}}(\vec{r},y';\omega)\hat{y}dy'$ with $\vec{\vec{G}}(\vec{r},\vec{r}';\omega)$ being the Green's function in the frequency domain given in Ref. 13. Here η is a positive infinitesimal number to ensure causality. We have collected all derivation details for Eq. (4) in the Appendix. In the limit of $\alpha \to \infty$, it is easy to verify that

$$H(\omega)|_{\alpha\to\infty} = \frac{2\pi\omega}{\alpha}\frac{1}{2\pi(\omega-\omega_0+i\eta)/\alpha} = \frac{\omega}{\omega-\omega_0+i\eta}. \tag{5}$$

Inserting Eq. (5) back into Eq. (3), we reproduce the previous result with the step function switching on [i.e., Eq. (1) of Ref. 15].

From previous studies for the 2D focusing,[15] we understand that the image oscillation is caused by the interference between the working frequency component, denoted symbolically by $E_0 e^{i\omega_0 t}$, and the transient surface mode at the upper band edge, denoted by $E_{\text{edge}} e^{i\omega' t}$.[15] The oscillation amplitude is roughly determined by $|E_{\text{edge}}/E_0|$, so that one can control the oscillation by tuning the edge state strength.[15] Certainly absorption can suppress the edge mode, but unfortunately it degrades the image resolution at the same time.[5] Here, we show that the present switching-on process offers us new possibilities to tune the strength of the transient edge mode, without affecting the working mode. Figure 1(b) shows the spectrum function $H(\omega)$ (with the working frequency $f_0=10$ GHz) versus frequency, with different values of α. It is clear that as α decreases, $H(\omega)$ becomes more localized around the working frequency at 10 GHz, so that the relative strengths for *other frequency components* are significantly suppressed. This is consistent with our naïve expectation—the smoother the switching on is, the less the induced transient modes are. In the limit of $\alpha \to 0$, namely the truly adiabatic switching-on process, we find that $H(\omega) \propto \delta(\omega-\omega_0)$ (see the Appendix), implying that no transient waves are induced at all.

We estimate the strengths of the edge mode (E_{edge}) and the working frequency mode (E_0), by calculating the integrand of Eq. (3), i.e., $|e^{-i\omega t}\vec{E}(\vec{r},\omega)H(\omega)|$, at the right frequencies. Following Ref. 15, we assume that $\varepsilon=\mu=1-200/f(f+i\gamma)$, yielding $\varepsilon(f_0)=\mu(f_0)\approx -1+i0.2\gamma$ at the working frequency $f_0=10$ GHz.[17] We have calculated E_{edge} and E_0 as the functions of α, and depict, in Fig. 2, $|E_{\text{edge}}/E_0|$ as a function of t_s/T_0 with different values of γ. Here $T_0=0.1$ ns is the time period of the working frequency. With a fixed α (or t_s/T_0), we note that $|E_{\text{edge}}/E_0|$ becomes larger with a smaller γ, which is consistent with previous observations that a smaller γ indeed yields a stronger oscillation.[8,15] On the other hand, we find that $|E_{\text{edge}}/E_0|$ becomes significantly reduced when the switching-on time becomes longer, especially when longer than a critical value $\sim 100T_0$. Thus the

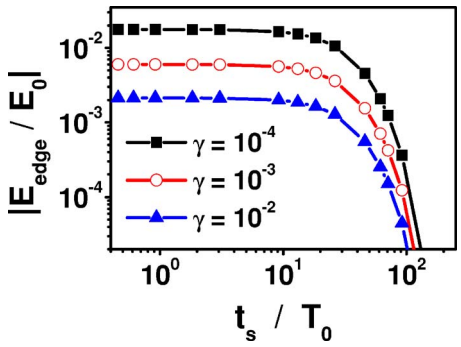

FIG. 2. (Color online) Calculated $|E_{edge}/E_0|$ as the functions of the switching-on time t_s with different values of γ (in units of GHz). Here $d=10$ mm.

oscillation could be significantly suppressed if we choose a longer switching-on time in the turning-on process. It is interesting to note that this critical value has a rather weak dependence on the value of γ.

In order to prove this idea, we employ the TDGF approach[15] to quantitatively evaluate $E(t)$ (at the image point) as the functions of time, with different fixed values of α, and show the results in Fig. 3(a). We see a strong field oscillation in the case of $\alpha=10$ GHz, but the oscillation is almost diminished in the case of $\alpha=0.8$ GHz. If we decrease the value of α further ($\alpha=0.2$ GHz), the oscillation is suppressed better and is essentially undetectable. However, we find that the global speed of relaxation toward stabilization is apparently slowed down, indicating that here the switching-on speed of the source is too slow to follow the

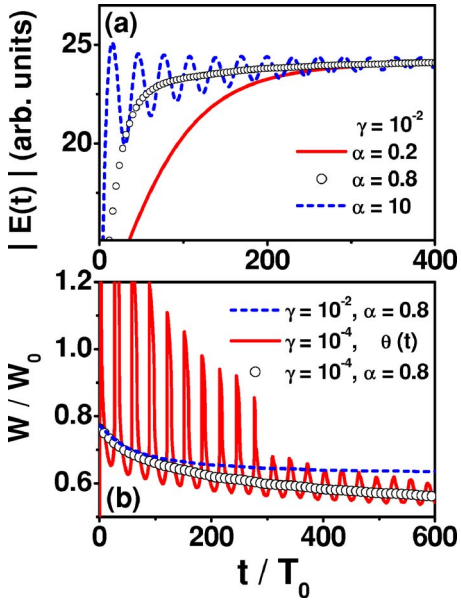

FIG. 3. (Color online) (a) Field amplitude (at the image point) as a function of time with different values of α (in units of GHz) and $\gamma=0.01$ GHz. (b) Image peak width as a function of time with $\gamma=10^{-4}$ GHz and $\alpha=0.8$ GHz (open circles), compared with the results calculated with $\gamma=10^{-2}$ GHz and $\alpha=0.8$ GHz (dashed line), and with $\gamma=10^{-4}$ GHz and a $\theta(t)$ switching on (solid line). Here $d=10$ mm.

response of the lens. Since the reason that the lens works and causes growth of the evanescent waves is the presence of the interface resonances,[18] the resonances and their Q factors are intimately tied to the time for the effects to stabilize, which is the *intrinsic response time* of the lens. Mapping our problem to a mechanical analogy, we find that the $\alpha=10$ GHz case corresponds to an "under-damped" oscillator, while the $\alpha=0.2$ GHz case is an "over-damped" one. Therefore, there must be an optimum value of α to critically match the lens' response time, at which the oscillation is just damped out while the global relaxation speed is not too much sacrificed. For the present system, numerical calculations suggest that $\alpha_c \approx 0.8$ GHz.

On the other hand, since the absorption is not increased here, we do *not* degrade the image resolution when suppressing the oscillation. In Fig. 3(b), we plot W/W_0 as the functions of time for different values of α and γ, where W is the peak width measured at half maximum of the image and W_0 the diffraction-limited value.[15] While the image peak width strongly oscillates as a function of time in the case of the $\theta(t)$ switching,[15] the oscillations *almost disappear* in the cases of $\alpha=0.8$ GHz independent of the values of γ. We note that the finally achieved image resolution strongly depends on γ, and a smaller γ yields a better resolution with a smaller W, as indicated in Fig. 3(b). This is because the surface waves that favor a higher image resolution increase as the losses decrease near the condition of $n=-1$, as discussed in Ref. 19. In viewing the results shown in Fig. 3, we conclude that we have established a mechanism to suppress the image oscillations, without increasing the absorption which degrades the resolution enhancement.

To better understand the influences of the switching-on time on the image formations, we show the evolutions of the image patterns in the turning-on processes with $\alpha=0.8$ GHz [Fig. 4(a)] and with a $\theta(t)$ switching on [Fig. 4(b)]. In the case of $\alpha=0.8$ GHz, we find that the image becomes sharper and sharper as time increases. On the other hand, when the switching-on process is a step function, we find the evolution of image formation is *not monotonic*, since the image pattern at $t=20$ ns is obviously sharper than that at $t=40$ ns.

III. THE ROLE OF THE SOURCE SPECTRUM

Previous studies revealed distinct image oscillation behaviors in different situations.[15,16] These complexities propose a challenging problem to realistic applications. It is then desirable to derive a general picture to understand the image oscillations in an arbitrary case. To achieve this goal, in this section, we will study several typical focusing problems, aiming to uncover the underlying physics behind the apparently different transient behaviors.

In what follows, without losing generality, we assume that

$$\varepsilon(f) = 1 - \frac{f_{pe}^2}{f(f+i\gamma)}, \quad \mu(f) = 1 - \frac{f_{pm}^2}{f(f+i\gamma)}, \tag{6}$$

with $f_{pe}^2=100(2+\delta), f_{pm}^2=100(2-\delta)$. At the working frequency $f_0=10$ GHz, we get $\varepsilon(f_0)\approx -1-\delta+i0.2\gamma, \mu(f_0)\approx$

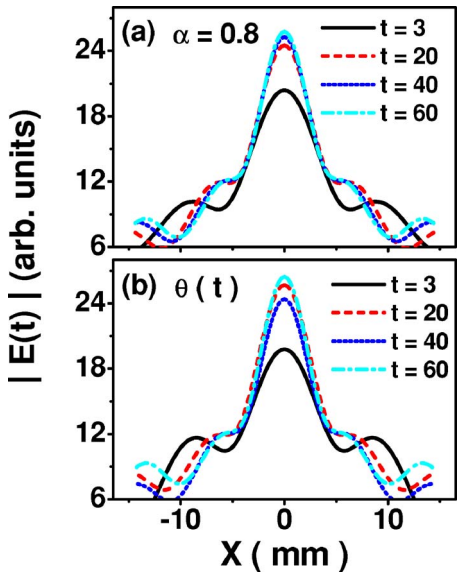

FIG. 4. (Color online) Image patterns (calculated with $y=0, z=-2d$) measured at different time instances as indicated in the legends, for focusing processes with $\alpha=0.8$ GHz (a) and with a step function switching on (b). Here $d=10$ mm, $\gamma=10^{-4}$ GHz.

$-1+\delta+i0.2\gamma$. In the remaining part of this paper, we fix $\gamma=10^{-3}$ GHz and only study the role of $\delta(\geqslant 0.2\gamma)$ played in such problems. We first check whether the metamaterial lens defined by Eq. (6) is still a super lens. For the three dimensional (3D) focusing geometry as described in Ref. 16, we employed the Green's function approach to calculate the resolution enhancement, $R=W_0/W$, for the finally stabilized image. Figure 5 depicts R as a function of the parameter δ. We find that "subwavelength" images (i.e., $R>1$) could indeed be formed when δ is sufficiently small, and the resolution enhancement depends logarithmically on the value of δ. More interestingly, we note that a super lens with $\varepsilon=-1-\delta, \mu=-1+\delta$ is even better than a super lens with $\varepsilon=\mu=-1-\delta$,[5,12,16] since the former yields a higher resolution enhancement than the latter with the same value of δ. This is simply because the refraction index is closer to the perfect lens value in the former lens $(n\rightarrow -1+\delta^2/2)$ than in the latter lens $(n\rightarrow -1-\delta)$.

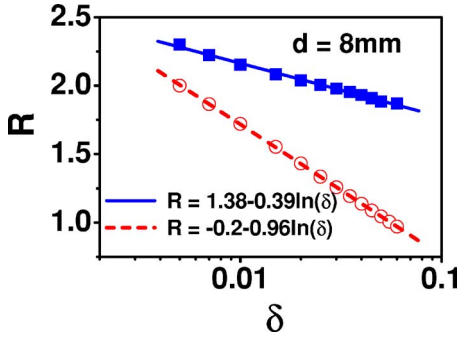

FIG. 5. (Color online) Resolution enhancement as a function of δ for metamaterial lenses with $\varepsilon=-1-\delta, \mu=-1+\delta$ (solid squares) and $\varepsilon=\mu=-1-\delta$ (open circles). Lines are the fitted results. Here the thickness of the lens is fixed as 8 mm.

Now that the proposed metamaterial lens is still a super one, we examine the transient behaviors associated with this type of lensing problems. We consider the following three typical types of source:

(1) 2D configuration with a line current source described by $\vec{J}^{2D}(\vec{r},t)=\hat{y}I_0\delta(x)\delta(z)e^{-i\omega_0 t}\theta(t)$;

(2) 3D configuration with a point current source polarized parallel to the lens plane, described by $\vec{J}^{3D_\parallel}(\vec{r},t)=\hat{y}P_0\delta(\vec{r})e^{-i\omega_0 t}\theta(t)$;

(3) 3D configuration with a point current source polarized perpendicular to the lens plane, described by $\vec{J}^{3D_\perp}(\vec{r},t)=\hat{z}P_0\delta(\vec{r})e^{-i\omega_0 t}\theta(t)$.

It is well known that the reflection and transmission coefficients for a slab are polarization, angular, and frequency dependent. As the sources considered here have related polarization, angular, and frequency dependencies, the combination of these source and scattering dependencies leads to many interesting physical effects, which will be illustrated below. It is worth noting that configurations (2) and (3) considered here are closely related to the famous Sommerfeld problem.[20]

As before,[15,16] here we assume the lens is placed parallel to the xy plane. We note that the above three configurations have covered *all* linearly independent situations, so that understanding their transient behaviors is crucial to understand a general problem, which may simply be a linear combination of them. Without introducing too many parameters, here we take the step function switching on. The mathematical formalisms for the first two cases have been recorded in Refs. 15 and 16. For the third case, we find the time-dependent **E** field should be calculated by Eq. (3) but with $\vec{E}(r,\omega)$ given by $\vec{E}(\vec{r},\omega)=-\mu_0 P_0\vec{G}(\vec{r},0;\omega)\cdot\hat{z}$. In explicit forms, we find that in the image region (see the definitions in Refs. 15 and 16), the z component of the E field is

$$E_z^{3D_\perp}(x,y=0,z;\omega) = -\frac{i\mu_0 P_0}{8\pi}\int \frac{k_\parallel^3}{(\omega/c)^2 k_{0z}} J_0(k_\parallel x) T^{TM}(k_\parallel,\omega) e^{-ik_{0z}z} dk_\parallel, \tag{7}$$

where $k_{0z}^2+k_\parallel^2=(\omega/c)^2$, $T^{TM}(k_\parallel,\omega)$ is the transmission coefficient for transverse-magnetic (TM) polarization, and J_0 is the usual Bessel function.

We employed the TDGF approach to quantitatively study the image formation processes in the above three cases. Solid lines in Fig. 6 show the calculated field amplitudes, measured at the image point, as the functions of time in all three cases. Here, we have set $\delta=0.05$ and $d=10$ mm. We find distinct image oscillation behaviors in different cases, even though the employed metamaterial lenses are *exactly* the same. Again, we find that the oscillation is induced solely by the evanescent waves, since no oscillation is observed if only propagating waves are considered.

To understand these intriguing transient behaviors, we study the surface wave (SW) spectrum of the present geometry, as the evanescent components of the source must couple to the surface modes of the slab lens. Shown in Fig. 7(a) is

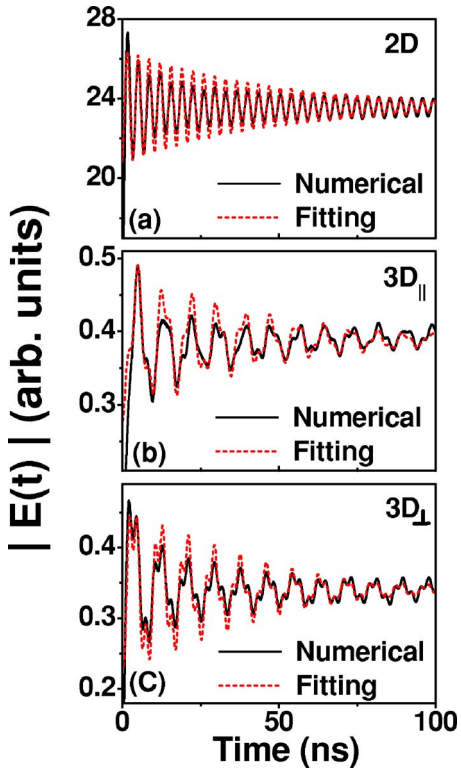

FIG. 6. (Color online) E-field amplitudes (at the image points) as the functions of time for three models explained in the text, calculated by the TDGF approach (solid lines) and the model fittings (dashed lines) described in the text.

the SW spectrum of the present system. Since we assume $\varepsilon \neq \mu$ in this paper, the spectra of the transverse-electric (TE) mode and the TM mode are well separated, in contrast to previous studies.[15,16] For an easy comparison explained later,

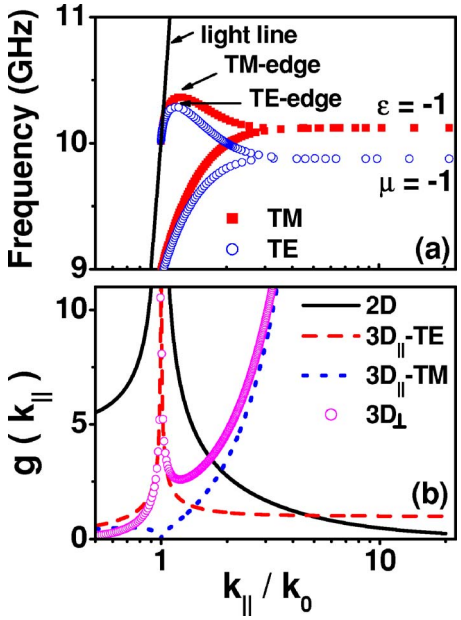

FIG. 7. (Color online) (a) SW dispersion relations for TE and TM polarizations. (b) Source spectrum $g(k_\parallel)$ as the functions of $k_\parallel$, in different cases.

here we scale the parallel k component, $k_\parallel$, by a constant $k_0 = \omega_0/c$ where ω_0 is the working frequency. From the SW spectrum, we can easily identify four states: (1) TE edge state, (2) $\mu=-1$ state, (3) TM edge state, (4) $\varepsilon=-1$ state. We note that the first two states are mainly determined by μ, while the last two are determined by ε.[21,22] Recalling that the SW density of state (DOS) is inversely related to the group velocity defined by $V_g = \partial\omega/\partial k_\parallel$, we see immediately that SW-DOS is very large at these four states. Since these four modes have large DOS and do not transport energy, once being excited in the switching-on process, they are difficult to damp out and thus will interfere with the working component to form complicated image oscillations. However, considering the fact the metamaterial lenses are exactly the same in all three cases, the question is then, why are the transient wave dynamics completely different in these three cases?

We find that the answer is associated with the source. The idea is quite simple—the nontransporting SW modes of the slab lens may *not* be excited if the employed source *does not* contain such a component. We now look at the problem in a more mathematical way. From Refs. 15 and 16 and Eq. (7), neglecting some trivial constants, we find that the transient wave component (at the image point, i.e., $x=0$) can be written as the following unified form:

$$E(\omega) \sim \int [g^{TE}(k_\parallel,\omega)T^{TE}(k_\parallel,\omega) + g^{TM}(k_\parallel,\omega)T^{TM}(k_\parallel,\omega)]e^{i2k_{0z}d}dk_\parallel, \tag{8}$$

where d is the lens thickness and $g(k_\parallel)$ is the spectrum function of the source, which determines how much the transient wave component is contained in the source. On the other hand, we note that $T(k_\parallel,\omega)$ are only determined by the lens, but have nothing to do with a concrete source. Straightforward calculations show that

$$g^{TE}_{2D}(k_\parallel,\omega) = \frac{1}{\sqrt{(\omega/c)^2 - k_\parallel^2}}, \quad g^{TM}_{2D}(k_\parallel,\omega) \equiv 0, \tag{9}$$

$$g^{TE}_{3D_\parallel}(k_\parallel,\omega) = \frac{k_\parallel}{\sqrt{(\omega/c)^2 - k_\parallel^2}}, \quad g^{TM}_{3D_\parallel}(k_\parallel,\omega) = \frac{k_\parallel\sqrt{(\omega/c)^2 - k_\parallel^2}}{(\omega/c)^2}, \tag{10}$$

$$g^{TE}_{3D_\perp}(k_\parallel,\omega) \equiv 0, \quad g^{TM}_{3D_\perp}(k_\parallel,\omega) = \frac{k_\parallel^3}{(\omega/c)^2\sqrt{(\omega/c)^2 - k_\parallel^2}}. \tag{11}$$

While symmetry requires strictly that $g^{TM}_{2D}(k_\parallel,\omega)\equiv 0$ and $g^{TE}_{3D_\perp}(k_\parallel,\omega)\equiv 0$, the spectrum functions in other cases are quite complicated and different, as shown in Fig. 7(b). We note from Fig. 7(a) that the edge states are very close to the light line at $k_\parallel=\omega/c$, while the $\varepsilon,\mu=-1$ states are located in $k_\parallel\to\infty$. Intuitive expectation suggests that, the edge states must become important if $g(k_\parallel)$ is large near $k_\parallel=\omega/c$, and the $\varepsilon,\mu=-1$ states become important when $g(k_\parallel)$ diverges as $k_\parallel \to \infty$.

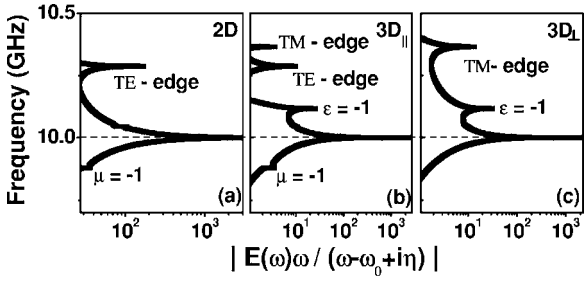

FIG. 8. Calculated integrand, $|E(\omega)\omega/(\omega-\omega_0+i\eta)|$, as the functions of frequency for three models.

To test this picture, we have quantitatively calculated the integrand function of Eq. (3) with $\delta=0.05$, $d=10$ mm, and $f_0=10$ GHz, and have shown the results in Figs. 8(a)–8(c) for three cases, respectively. We first note that, beside the common working component, the 2D configuration only excites two TE transient modes and the $3D_\perp$ configuration only excites two TM ones, in consistency with the symmetry restrictions discussed above. When we examine the 2D case [Fig. 8(a)] more carefully, we find that the TE edge mode is much stronger than the $\mu=-1$ state. This is quite intriguing at first sight, since the latter is actually *closer* to the working frequency. The reason can be traced to the spectrum function of the 2D source, which diverges at $k_\parallel=\omega/c$ but decays to zero as $k_\parallel\to\infty$ [Fig. 7(b)]. This naturally explains why the TE edge state is much stronger than the $\mu=-1$ state in this case.

We now check the $3D_\perp$ case shown in Fig. 8(c). Since the source spectrum diverges at both $k_\parallel=\omega/c$ and $k_\parallel\to\infty$ [Fig. 7(b)], we find the TM edge state and the $\varepsilon=-1$ state contribute *nearly equally* importantly, in sharp contrast to the 2D case.

The most complicated situation is the $3D_\perp$ case shown in Fig. 8(b), where all four transient modes are excited. However, we find that the TE edge mode is much stronger than the TM edge mode, and the $\varepsilon=-1$ state is much stronger than the $\mu=-1$ state. This is surprising at first sight, since one naively expects a good symmetry between the TE and the TM modes (remembering that $\varepsilon\approx\mu$ here).[21,22] The physics is again governed by the source spectrum, which distinguishes the TE and TM polarizations. From Fig. 7(b), we understand that, while $g_{3D_\perp}^{TE}(k_\parallel)$ diverges at $k_\parallel=\omega/c$ and decreases to a small value as $k_\parallel\to\infty$, $g_{3D_\perp}^{TM}(k_\parallel)$ behaves just on the opposite. Due to such an asymmetry in the source spectrum, the system only picks up the TE edge and the $\varepsilon=-1$ states as the dominant transient waves.

Based on the above arguments, we fit the field oscillations using the following formula:

$$|E(t)| = \left| E_0 e^{i\omega_0 t} + \sum_j E_j e^{i\omega_j t} \right| e^{-\beta t}, \tag{12}$$

where E_0 is the strength of the working frequency component at ω_0, $\{E_j\}$ are the transient components at ω_j, and β is the damping rate. In our fittings, besides the working mode, we have taken one transient component (the TE edge state) for the 2D case, two (the TE edge and the $\varepsilon=-1$ states) for the $3D_\parallel$ case, and two (the TM edge and the $\varepsilon=-1$ states) for the $3D_\perp$ case. Adjusting the parameters of those modes, we have obtained the best fitting results for all three models, and have shown them in Fig. 6 as dashed lines. Compared with the direct numerical results, the good agreement justifies the picture that we have presented.

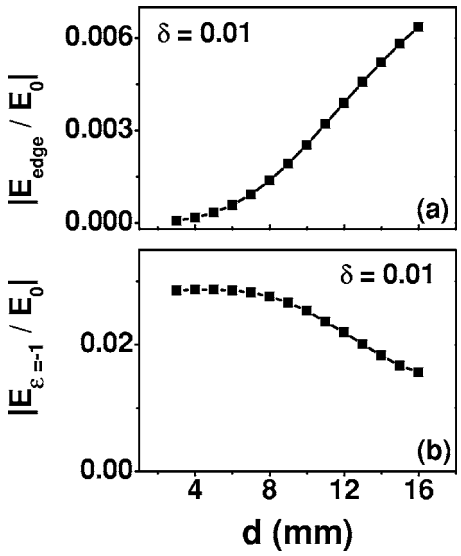

FIG. 9. (a) $|E_{edge}/E_0|$ and (b) $|E_{\varepsilon=-1}/E_0|$ as the functions of d. Here we set $\delta=0.01$.

IV. THE ROLES OF THE LENS PARAMETERS

We now study how the image oscillations depend on the properties of the lenses, including the metamaterial parameter δ and the slab thickness d. We take the $3D_\perp$ focusing case as an example to illustrate the main physics. As we have understood that the TE edge and the $\varepsilon=-1$ states play important roles in forming the transient-wave dynamics, we now examine how the strengths of these two states, denoted respectively, by E_{edge} and $E_{\varepsilon=-1}$ and represented by the peak values of the corresponding modes as shown in Fig. 8(b), be tuned by the parameters δ and d.

We first study the effect of d. Shown in Figs. 9(a) and 9(b) are $|E_{\text{edge}}/E_0|$ and $|E_{\varepsilon=-1}/E_0|$ as the functions of d, with $\delta=0.01$. We find that $|E_{\text{edge}}/E_0|$ is an increasing function of d while $|E_{\varepsilon=-1}/E_0|$ is a decreasing one. We also note that the thickness dependence of the edge state is much stronger than that of the $\varepsilon=-1$ state. These features can be understood from the SW spectrum. In a thicker lens, the edge state is closer to the working frequency so that its strength becomes stronger (remembering that $H(\omega)$ becomes larger approaching ω_0). On the other hand, the thickness dependence of the $\varepsilon=-1$ state is much less significant, since the position of the $\varepsilon=-1$ state in the SW spectrum is solely determined by the intrinsic properties of the metamaterials, but does not depend on the lens thickness d at all.

We next study the effect of δ. Fixing $d=10$ mm, we have calculated $|E_{\text{edge}}/E_0|$ and $|E_{\varepsilon=-1}/E_0|$ as the functions of δ, and have shown the results in Figs. 10(a) and 10(b), respectively. We find the δ dependences of the two states are just

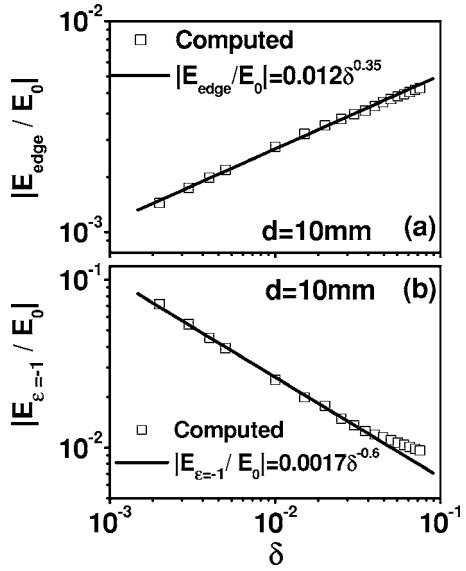

FIG. 10. (a) $|E_{edge}/E_0|$ and (b) $|E_{\varepsilon=-1}/E_0|$ as the functions of δ. Here we set $d=10$ mm. Solid lines are the fitting results employing power-law functions.

opposite to the corresponding d dependences, that is, the $\varepsilon=-1$ state becomes important as δ decreases while the edge state becomes less important. Again, these features can be understood from the SW spectrum. When δ decreases, the $\varepsilon=-1$ state is closer to the working frequency, so that its strength is enhanced significantly. For the edge state, although its own absolute strength (i.e., E_{edge}) is nearly independent of δ, its relative strength decreases since the working mode strength (i.e., E_0) is strongly enhanced as $\delta\to 0$ (approaching the perfect lens condition[2]). Numerical calculations suggest that both $|E_{\text{edge}}/E_0|$ and $|E_{\varepsilon=-1}/E_0|$ exhibit power law dependence on δ in the studied parameter regime, as shown by the solid lines in Figs. 10(a) and 10(b). However, we emphasize that the power relation for $|E_{\varepsilon=-1}/E_0|$ does not hold when δ is very close to 0, in which case we can no longer separate the $\varepsilon=-1$ state from the working mode.

Simply speaking, the oscillation contributed by the edge mode is more sensitive to the changes of the lens thickness d, while the oscillation contributed by the $\varepsilon=-1$ state is more sensitive to the changes of material parameter δ. With the knowledge of the dependences of $|E_{\text{edge}}/E_0|$ and $|E_{\varepsilon=-1}/E_0|$ on d and δ known from Figs. 9 and 10 one can easily predict the image oscillations of a given focusing problem before performing complicated calculations, and can efficiently tune the oscillatory behaviors via changing the values of d and δ.

V. CONCLUSIONS

To summarize, we have systematically studied the transient wave behaviors in metamaterial focusing. Adopting a model as general as possible, we have analyzed the image instabilities in different situations, and have identified three key factors that predominantly influence the transient-wave dynamics. These factors are the switching-on time, the source spectra, and the lens parameters. The obtained results form a unified framework to understand the complicated image instability phenomena in different situations, and offer us the possibility to handle the image oscillations in practice. For example, we show that there exists an optimum value of switching-on time, with which the image oscillations can be significantly suppressed while the relaxation speed is not greatly sacrificed. More importantly, to achieve this effect, we do not need to increase the absorption rate of the lens, which may sadly degrade the image resolution. We also show that, the two types of transient modes that cause the image instabilities, can be respectively modulated by the lens thickness and the metamaterial parameters.

ACKNOWLEDGMENTS

This work was supported by the National Basic Research Program of China (Grant No. 2004CB719800), NSFC (Grants No. 10504003 and No. 10321003), Shanghai Science and Technology Committee (Grants No. 05PJ14021 and No. 05JC14061), Fok Ying Tung Educational Foundation, and PCSIRT. C.T.C. thanks support from NSFC (Grant No. 10229402).

APPENDIX: DERIVATION OF EQ. (4)

In this Appendix, we present the derivation details of Eq. (4). According to Eq. (2), we obtain

$$\vec{J}(\vec{r},t)=\hat{y}I_0\delta(x)\delta(z)e^{-i\omega_0 t}\left[\frac{\alpha e^{-\alpha t}}{(1+e^{-\alpha t})^2}-\frac{i\omega_0}{(1+e^{-\alpha t})}\right]. \tag{A1}$$

Based on the TDGF approach,[15] we find that

$$\begin{aligned}H(\omega)&=\int e^{i(\omega-\omega_0+i\eta)t'}\left[\frac{\alpha e^{-\alpha t'}}{(1+e^{-\alpha t'})^2}-\frac{i\omega_0}{(1+e^{-\alpha t'})}\right]dt'\\&=-i(\omega-\omega_0+i\eta)\int\frac{e^{i(\omega-\omega_0+i\eta)t'}}{(1+e^{-\alpha t'})}dt'\\&\quad-i\omega_0\int\frac{e^{i(\omega-\omega_0+i\eta)t'}}{(1+e^{-\alpha t'})}dt'=-i\omega\int\frac{e^{-i(\omega-\omega_0+i\eta)t'}}{(1+e^{\alpha t'})}dt'.\end{aligned} \tag{A2}$$

Define a function of complex variable as

$$f(z)=e^{-i(\omega-\omega_0+i\eta)z}.\frac{1}{1+e^{\alpha z}}, \tag{A3}$$

what we need is to calculate the following integration:

$$I=\int_{-\infty}^{+\infty}f(x)dx \tag{A4}$$

along the real axis. We note that $f(z)$ has an infinite series of single poles at $z_k=i(2k+1)\pi/\alpha$, and that $f(z+2\pi i/\alpha)=e^{2\pi(\omega-\omega_0+i\eta)/\alpha}f(z)$. Let us define a closed path in the complex plane: $l_1:(-a,0)\to(a,0)$; $l_2:(a,0)\to(a,2\pi/\alpha)$; $l_3:(a,2\pi/\alpha)\to(-a,2\pi/\alpha)$; $l_4:(-a,2\pi/\alpha)\to(-a,0)$. The integration along this loop yields

$$\oint_l f(z)dz = \int_{-a}^{a} f(z)dz + \int_{l_2} f(z)dz + e^{2\pi(\omega-\omega_0+i\eta)/\alpha}\int_{a}^{-a} f(z)dz + \int_{l_4} f(z)dz. \tag{A5}$$

In the limit of $a\to\infty$, we can easily demonstrate that the second and the fourth integrations are both zero. On the other hand, the loop integration in the left-hand side of Eq. (A5) can be worked out based on the residue theorem. Collecting terms, we obtain

$$2\pi i\cdot\left[-\frac{e^{\pi(\omega-\omega_0+i\eta)/\alpha}}{\alpha}\right] = [1-e^{2\pi(\omega-\omega_0+i\eta)/\alpha}]I \tag{A6}$$

with which we arrive at the desired result,

$$H(\omega) = \frac{2\pi\omega}{\alpha}\cdot\frac{e^{-\pi(\omega-\omega_0+i\eta)/\alpha}}{1-e^{-2\pi(\omega-\omega_0+i\eta)/\alpha}}. \tag{A7}$$

In the limit of $\alpha\to 0$, Eq. (A2) becomes

$$H(\omega)_{\alpha\to 0} = -i\omega\int\frac{e^{-i(\omega-\omega_0+i\eta)t'}}{2}dt' = -i\omega\pi\delta(\omega-\omega_0). \tag{A8}$$

*Author to whom correspondence should be addressed. Email address: phzhou@fudan.edu.cn

[1] V. C. Veselago, Sov. Phys. Usp. **10**, 509 (1968).
[2] J. B. Pendry, Phys. Rev. Lett. **85**, 3966 (2000).
[3] N. Garcia and M. Nieto-Vesperinas, Phys. Rev. Lett. **88**, 207403 (2002).
[4] J. B. Pendry, Phys. Rev. Lett. **91**, 099701 (2003).
[5] D. R. Smith, D. Schurig, M. Rosenbluth, S. Schultz, S. A. Ramakrishna, and J. B. Pendry, Appl. Phys. Lett. **82**, 1506 (2003).
[6] R. W. Ziolkowski and E. Heyman, Phys. Rev. E **64**, 056625 (2001).
[7] X. S. Rao and C. K. Ong, Phys. Rev. B **68**, 113103 (2003).
[8] X. S. Rao and C. K. Ong, Phys. Rev. E **68**, 067601 (2003).
[9] S. A. Cummer, Appl. Phys. Lett. **82**, 1503 (2003).
[10] P. F. Loschialpo, D. L. Smith, D. W. Forester, F. J. Rachford, and J. Schelleng, Phys. Rev. E **67**, 025602(R) (2003).
[11] L. Chen, S. He and L. F. Shen, Phys. Rev. Lett. **92**, 107404 (2004).
[12] R. Merlin, Appl. Phys. Lett. **84**, 1290 (2004).
[13] Y. Zhang, T. M. Grzegorczyk, and J. A. Kong, Electromagn. Waves **35**, 271 (2002).
[14] G. Gomez-Santos, Phys. Rev. Lett. **90**, 077401 (2003).
[15] L. Zhou and C. T. Chan, Appl. Phys. Lett. **86**, 101104 (2005).
[16] L. Zhou and C. T. Chan, Opt. Lett. **30**, 1812 (2005).
[17] We note that this form of ε and μ corresponds to a special case (with δ=0) of the general form of Eq. (6). We adopt this form here because the resulting image oscillation is the simplest, so that the role of switching-on time can be illustrated more clearly. We have studied the case with a nonzero δ, and found that the qualitative conclusions remain unchanged.
[18] A. Alu and N. Engheta, IEEE Trans. Antennas Propag. **51**, 2558 (2003).
[19] A. Ishimaru, J. R. Thomas, and S. Jaruwatanadilok, IEEE Trans. Antennas Propag. **53**, 915 (2005).
[20] A. N. Sommerfeld, Ann. Phys. **81**, 1135 (1926).
[21] R. Ruppin, J. Phys.: Condens. Matter **13**, 1811 (2001).
[22] L. Zhou and C. T. Chan, Appl. Phys. Lett. **84**, 1444 (2004).